Dislocation onset and nearly axial glide in carbon nanotubes under torsion

D.-B. Zhang,[1] R. D. James,[2] and T. Dumitrică[1,a)]
[1]*Department of Mechanical Engineering, University of Minnesota, Minneapolis, Minnesota 55455, USA*
[2]*Department of Aerospace Engineering and Mechanics, University of Minnesota, Minneapolis, Minnesota 55455, USA*

(Received 9 December 2008; accepted 26 January 2009; published online 19 February 2009)

The torsional plastic response of single-walled carbon nanotubes is studied with tight-binding objective molecular dynamics. In contrast with plasticity under elongation and bending, a torsionally deformed carbon nanotube can slip along a nearly axial helical path, which introduces a distinct $(+1,-1)$ change in wrapping indexes. The low energy realization occurs without loss in mass via nucleation of a 5-7-7-5 dislocation dipole, followed by glide of 5-7 kinks. The possibility of nearly axial glide is supported by the obtained dependence of the plasticity onset on chirality and handedness and by the presented calculations showing the energetic advantage of the slip path and of the initial glide steps. © *2009 American Institute of Physics*.
[DOI: 10.1063/1.3081627]

The remarkable physical properties of carbon nanotubes (CNTs) originate in their objective atomic structure[1] where each carbon atom sees precisely the same environment up to rotation and translation. Modulating these properties is highly desirable for various applications and systematic ways to manipulate the perfect arrangement of hexagonal rings are needed. A wealth of experimental data[2] shows that the near-sublimation thermal agitation does not necessarily destroy CNTs. Instead, it can have a positive effect, especially when combining the significant random agitation of the atoms with a coherent component caused by an externally applied deformation. For example, recent experiments on superplasticity[3,4] obtained that CNTs under tensile load can undergo large elongation and thinning without abandoning their perfection. Theoretical studies[5–7] indicated that superplasticity relies on primary microscopic mechanisms, like a mass-conserving glide along a helical slip path, as well as on a nearly axial kink propagation with dimers directly breaking out of the lattice. Remarkably, each mass-conserving glide step lowers the CNT diameter and changes its index from (n,m) to $(n,m-1)$ or $(n-1,m)$. Plasticity under bending[8,9] was also described in terms of kink motion along a helical path.

What other primary transformations can be induced by external deformation on the hot CNT lattice? To address this question we considered CNT plasticity under another fundamental type of deformation—*torsion*. Due to recent experimental advances,[10–12] it is now possible to probe CNTs as torsional springs. The popular atomistic modeling tools are unsuitable for modeling this type of deformation. Relying on recent theoretical innovations,[13,14] we describe the CNT's torsional response with objective molecular dynamics (MD) and predict the possibility of a new mass-conserving nearly axial glide. Such glide cannot be promoted by pure tension. We first indicate by direct calculation the susceptibility of twisted (n,m) CNTs to the new slip path. Next, we show that the practical realization can be largely accomplished without the need of preexisting defects as it can be triggered by the nucleation of a 5-7-7-5 dislocation dipole. Once nucleated, the 5-7 kinks glide away from each other, leaving behind an $(n+1,m-1)$ CNT.

Objective MD represents a generalization of the widely used MD under periodic boundary conditions (PBCs). In PBC MD, the solution satisfies the specified translational invariance of a CNT. In objective MD, the helical symmetry of a CNT is no longer concealed and the solution is invariant to the specified helical group operations of a CNT. Here, we describe an infinitely long CNT with

$$\mathbf{X}_{i,\zeta} = \mathbf{R}^{\zeta}\mathbf{X}_i + \zeta\mathbf{T}. \tag{1}$$

Index i runs over the N_0 atoms at locations $\mathbf{X}_i$ inside the objective simulation domain, which in general is different from the PBC one, and index ζ labels the various domain replicas. Rotational matrix $\mathbf{R}$ of angle θ and the axial vector $\mathbf{T}$ characterize the helical transformations applied to the objective domain. Given the objective domain, the θ_0 value for a strain-free (n,m) CNT has analytical form.[13] Note that objective MD has been previously applied to study linear elasticity as well as torsional and bending instabilities of CNTs.[13,15] Here we show a new utility in the context of plasticity and defect glide.

Atomistic simulations based on empirical potentials have been carried out recently on the torsional response of CNTs.[16–19] To minimize the magnitude of the end effects introduced by the employed cluster representation of a realistic micrometer-long CNT, as well as the influence on the strain energy caused by the additional kinematic constraints introduced by fixed boundary conditions, accounting for a large number of atoms was necessary. The widely used PBC MD avoids the spurious end and fixed boundary effects but requires large translational cells or supercells and can describe only discrete torsional deformations compatible with the assumed translational symmetry.[20] The advantage of ob-

a)Author to whom correspondence should be addressed. Electronic mail: td@me.umn.edu.

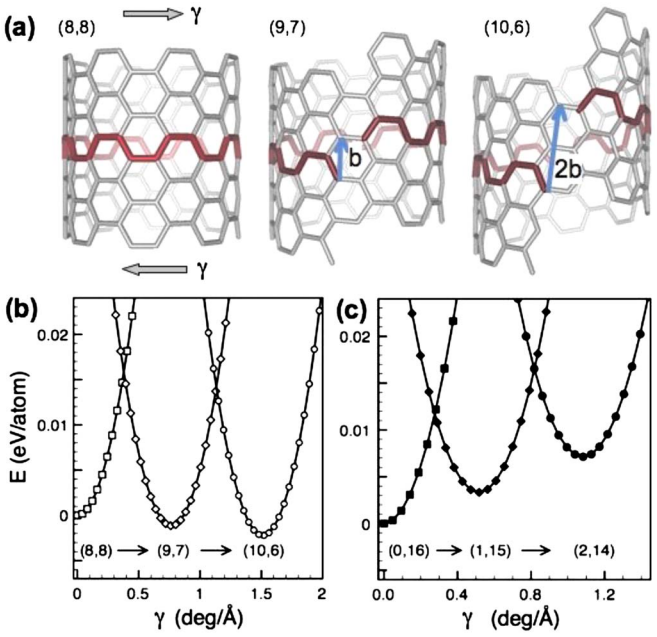

FIG. 1. (Color online) (a) Objective MD cells shown in red (dark) for (8,8), (9,7), and (10,6) CNTs, all contain 32 atoms. Screw vectors **b** and 2**b** specify the slip steps. Horizontal arrows show the right-handed applied twist. Strain energy vs the applied-twist rate starting from (b) armchair and (c) zigzag CNTs. The energy minima correspond to the strain-free CNTs of indexes indicated under each curve.

jective MD is that it treats on the same footing chirality and torsional deformations and thus can model chiral CNTs under *arbitrary* torsional distortion from relatively small objective domains. The introduced simplifications in the number of atoms allows us to apply an accurate, quantum-mechanical treatment of the chemical binding.[14] We employ the nonorthogonal two-center tight-binding (TB) model of carbon[21] as implemented in the computational package TROCADERO.[22] This microscopic model describes well the CNT mechanics.[15] To accommodate the objective boundary conditions (1), the TB electronic states were represented in terms of symmetry-adapted Bloch sums.[14] Between 5 and 100 uniformly distributed helical k-points were used to converge the band energy.

It is common to represent the CNT's translational, rotational, and helical symmetry with vectors in the unrolled representation projected onto a graphene sheet. Screw vectors have components along translational and circumferential vectors. The three Burgers vectors of graphene[4] indicate three nonequivalent helical slip paths for CNTs. We will show with direct objective MD calculations that the path indicated by the screw Burgers vector **b** with the smallest component in the circumferential direction is desirable under twist. At the same time, these calculations serve as a useful illustration of how the method works.

For right-handed CNTs, $\mathbf{b}=\mathbf{a}_1-\mathbf{a}_2$, where $\mathbf{a}_1$ and $\mathbf{a}_2$ are graphene lattice vectors. It is easy to see that a slip step achieved by a global network motion has the effect of changing the (n,m) CNT circumference vector from $\mathbf{C}=n\mathbf{a}_1+m\mathbf{a}_2$ to $\mathbf{C}'=\mathbf{C}+\mathbf{b}=(n+1)\mathbf{a}_1+(m-1)\mathbf{a}_2$, thus leading to $(n+1,m-1)$ CNT. For example, starting from (8,8) CNT, Fig. 1(a), glide with **b** and 2**b**, leads to (9,7) and (10,6) CNTs, respectively. The (8,8) CNT of Fig. 1(a) is described from the 32-atom translational domain shown with red (dark gray). Thus, in Eq. (1) **R** is the identity matrix ($\theta_0=0$) and index i runs over the atoms located in the translational domain of periodicity **T**. Once the stress-free configuration was identified through conjugate gradient potential energy scans under different $|\mathbf{T}|$ values, a torsional strain rate $\gamma=(\theta-\theta_0)/|\mathbf{T}|$ was imposed. The procedure was repeated for (9,7) and (10,6) CNTs, both described from the 32-atom domain altered by **b** and 2**b** slip steps, respectively.

The diameter- and length-conserving nearly axial glide does not bring any energetic advantage under tension. However, as it can be seen from the strain energy [measured with respect to the energy of (8,8) CNT] versus γ presented in Fig. 1(b), the situation is different under torsion. Starting from left, one sees the expected quadratic increase. Beyond a 0.4 deg/Å twist rate the armchair structure becomes unfavorable against the reversely twisted (9,7) CNT. As γ is further increased, the (9,7) CNT's strain energy decreases until the strain-free state is reached beyond which this CNT is forwardly twisted. Eventually (9,7) CNT looses its advantage to (10,6) CNT and so on until zigzag (16,0) CNT is obtained after 8**b** (not shown). Similar calculations presented in Fig. 1(c) started from the zigzag case show that the vertical glide introduces a change in handedness. The (16,0) CNT was represented as (0,16) CNT from a 32-atom domain with a $-8\mathbf{b}$ slip and $\theta_0=-11.25°$, which is the new reference value for measuring γ. Under twist (1,15) CNT ($-7\mathbf{b}$ slip left handed) becomes quickly favorable, followed by (2,14) CNT ($-6\mathbf{b}$ slip, left handed), and so on, until (8,8) CNT is regained.

The next logical step is to investigate the realization of the glide through discrete dislocation motion rather than by the unlikely motion of the graphene strip edges past one another. It is natural to conjecture nucleation of a primary Stone–Wales (SW) defect with two 5-7 dislocation cores (kinks) of $\pm\mathbf{b}$ Burgers vector. The importance of the SW defect in CNT plasticity under tension and bending is well recognized[8,9,23–25] but its role under torsion was not revealed.

In a pristine CNT, SW defect forms via a 90° bond flip. The encountered energy barrier is high[24,25] and the transformation requires high temperatures or irradiation. Notably, the SW defect structure is slightly elongated along the direction given by the pentagons. In the tubular geometry, the SW transformation of a noncircumferential or a nonaxial bond locally twists and lengthens the CNT. If the CNT is under torsion, a properly oriented defect can relive strain and eventually make the SW defected state energetically favorable over the pristine one. For example, the calculations presented in Fig. 2(a) show the energy dependence on the twist rate for the perfect and SW-defected (16,0) CNT. The minimum of the SW curve gives the twists rate $\gamma_{SW}=0.17$ eV/Å and formation energy $E_{SW}=4.0$ eV. The intersection of the two curves gives the critical twist rate $\gamma^*=0.72$ eV/Å above which the defected state becomes energetically favorable.

We now focus on the χ-dependence of the plasticity onset. Generally, in a chiral CNT there are three sets of nonequivalent bonds, labeled 1, 2, and 3 in Fig. 2(b), that make distinct angles β with respect to the CNT axis. Depending on the bond to undergo the SW transformation, there are three

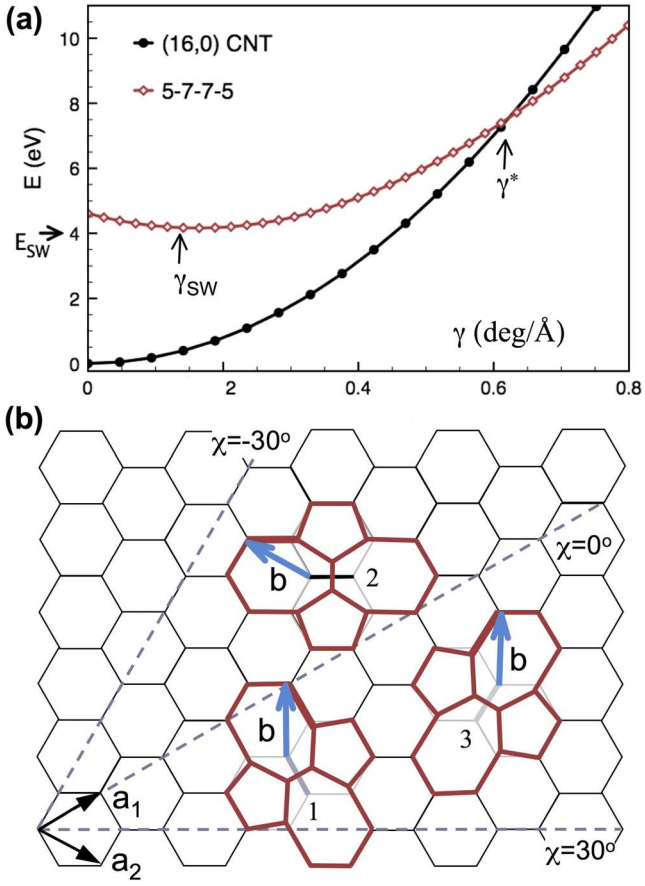

FIG. 2. (Color online) (a) Strain energy vs applied-twist rate for a perfect and SW defected (16,0) CNT. The simulation cell contains 128 atoms and it is derived from the translational cell of an (8,8) CNT via $-8\mathbf{b}$ slip steps. (b) Schematics of the nonequivalent 5-7-7-5 dislocation dipoles formed by 90° rotation of the three nonequivalent bonds labeled 1, 2, and 3. In (a), bond 2 underwent the SW transformation. Under twist, a 5-7 core can glide along the Burgers screw vector $\mathbf{b}$ shown in blue (light gray) via a 90° rotation of the adjacent shoulder bond. Chirality is measured by the angle χ made by projected circumference with graphene lattice vector $\mathbf{a}_1$. Thus, dashed lines indicate the armchair ($\chi=\pm 30°$) and zigzag ($\chi=0°$) directions.

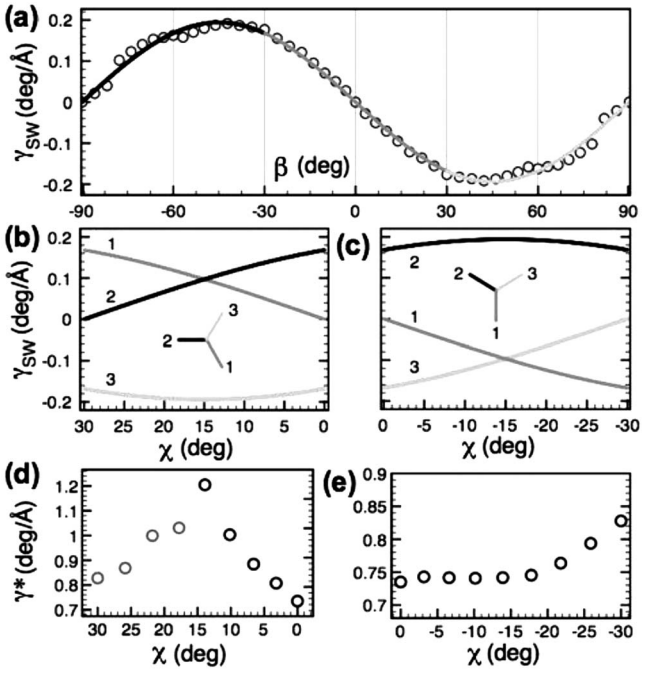

FIG. 3. (a) The twist rate γ_{SW} introduced by the SW transformation of a bond that initially makes an angle β with respect to the CNT axis. Calculations (open circles) were carried out on the [(8,8), (9,7),…, (16,0)] CNT family described from 128-atom objective domains. The continuous line is the fitting to lowest order in β. The reduced-zone representation, i.e., γ_{SW} as a function of chirality, in (b) right- and (c) left-handed CNTs. The three branches 1, 2, and 3 correspond to the three distinct bonds in a CNT shown in the schematics in the armchair and zigzag orientations. Plasticity onset as a function of chirality in (d) right- and (c) left-handed CNTs.

possible nonequivalent defect orientations. Given an applied twist handedness, the most likely bond to flip is the one that produces the largest γ_{SW} and thus the smallest γ^*. We have carried out a series of SW calculations for a series of nearly equal 5.8 Å in radius CNTs: (8,8), (9,7),…, (15,1), and (16,0), all described with the 128-atom translational supercell of the (8,8) CNT, as altered by the $0,\mathbf{b},\ldots,8\mathbf{b}$ slip steps, respectively. Relying of the objective MD capability of allowing an arbitrary twist, we were able to quantify γ_{SW} and then determine[26] γ^*. Calculations obtained $E_{SW}=4.04\pm0.5$ eV and a distinct β-dependence for γ_{SW}, as evidenced by Fig. 3(a). Fitting this atomistic data to the lowest order in β we have $\gamma_{SW}/[\text{deg/Å}]=-0.19\sin(2\beta)$.

More understanding can be gained by examining the added "reduced-zone" plots that present γ_{SW} introduced by the three distinct sets of bonds in a CNT of chirality χ. As χ varies from armchair to zigzag in right-handed CNTs, Fig. 3(b), our data shows that at $\chi=15°$ the bond most prone to the SW flip changes from 1 to 2. When going from zigzag to armchair (left-handed CNTs indicated by negative χ), Fig. 2(c), only bond 2 can be flipped by the applied twist. Note that the bonds identified here do not generally coincide with the ones prone to flip under external elongation.[24] The obtained χ-dependence for the onset of plastic deformation is correlated with the pronounced angular dependence of γ_{SW}. For right-handed CNTs, Fig. 3(d), the γ^* dependence indicates that the thermodynamic conditions for plastic yield are met latest at $\chi\sim15°$, where a crossover-cusp dependence is noted due to the change in the most favorable bond choice. For left-handed CNTs, Fig. 3(e), the dependence is smooth and bounded by the 0.7–0.85 deg/Å interval.

Once nucleated, SW defect splits into two 5-7 kinks via a succession of 90° bond flips.[6] Notably, in a twisted (n,m) CNT the split can occur in a distinct way, such that the kinks move along the Burgers vector directions indicated in Fig. 2(b) to leave behind an $(n+1,m-1)$ CNT region. We demonstrate the initial stages of glide by direct calculations carried out on (8,8) and (16,0) CNT described with an objective supercell containing 256 atoms. The bond to undergo the initial SW rotation was selected, as indicated by Fig. 3.

Figure 4(a) shows the topology of the SW defect obtained by the rotation of bond 1 in a (8,8) CNT, followed by the two initial stages of the glide process, as well as the energy dependence with the applied twist rate for these configurations. Several important features can be noted. All curves appear to have similar curvatures but their minimum points are shifted toward higher strain rate values. Additionally, the formation energy of the second glide step did not increase much compared to the first. As a result, the configurations with more glide steps are intersecting the pristine

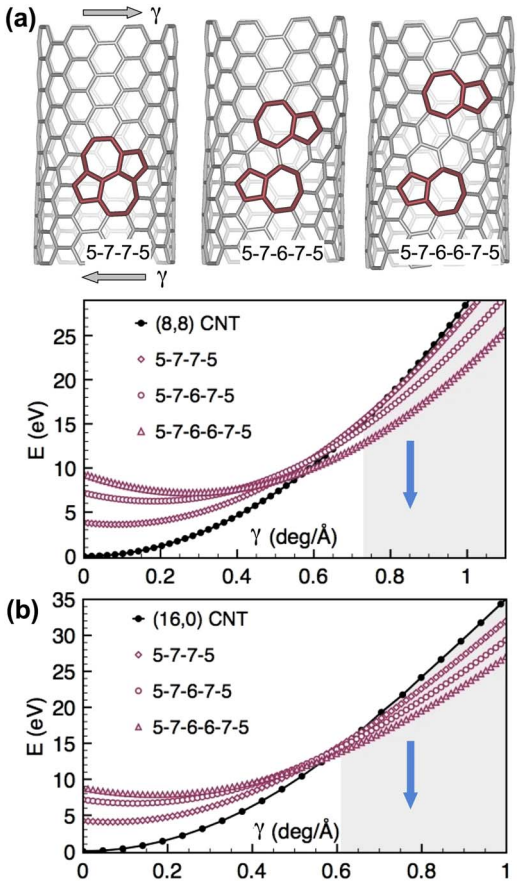

FIG. 4. (Color online) (a) Above: splitting of the 5-7-7-5 defect with axial glide of the 5-7 kink in (8,8) CNT under torsion. The first (5-7-6-7-5) and second (5-7-6-6-7-5) glide step configurations are shown. Below: energy vs applied twist rate for the pristine, SW defected, first, and second glide steps. Shaded area indicates the strain range where all defected CNTs become energetically favorable over the pristine one. The down arrow indicates the possibility of glide through the lower energetic states toward the (9,7) CNT. (b) Energy vs applied twist rate for the pristine (16,0) CNT, SW defected (bond 2), and first, second glide steps along the nearly axial glide direction.

(8,8) CNT curve earlier than the ones with fewer. By the time crossover of the SW curve with the pristine one occurs at 0.73 deg/Å, all following glide states would be lower in energy and the (8,8) CNT lattice can slide down through a series of glide steps toward energetically preferred (9,7) CNT. The same mechanism emerges from Fig. 4(b), demonstrating the nearly axial glide in (16,0) CNT.

In conclusion, relying on recent theoretical advances[13,14] that cast aside the translational symmetry of MD and consider instead the helical symmetry for both the electronic and ionic degrees of freedom, we were able to study the plasticity of single-walled CNTs under torsion. We found that the onset of plasticity depends not only on chirality but also on handedness. For a given handedness of the applied twist, chiral tubes of opposed handedness are most susceptible to yield. Remarkably, SW defect nucleation and strain-driven kink motion emerge as a universal plastic mode in CNTs. While under elongation and bending, kink glide is restricted to pure helical glide paths, torsion makes possible the mass-conserving kink glide along the most axially oriented path. The resulting chirality transformation allows spanning the 0°–30° chirality range via a collection of nearly constant-radius CNTs and thus opens the interesting possibility of modulating the CNT electronic properties without affecting stability.

In general, motion of the 5-7 kink is associated with chirality and length changes while an isolated pentagonal (heptagonal) ring produces positive (negative) curvature and incurs extended shape changes like bending. Very often such transformations are incompatible or inconveniently described with translational symmetry. Because the space of available deformations[13] is larger than in PBC MD, objective MD appears an interesting method for further studies of plasticity and motion of defects in CNTs and other objective structures.

Work supported by AFOSR (Computational Mathematics, Dr. Fariba Fahroo). D.-B.Z. and T.D. thank NSF CAREER (Grant No. CMMI-0747684) and Donors of the American Chemical Society Petroleum Research Fund for supporting this work. R.D.J. acknowledges support from AFOSR (GameChanger, Grant No. GRT00008581/RF60012388), NSF (Grant No. DMS-0757355), and DOE (Grant No. DE-FG02-05ER25706). Computations were carried out at the Minnesota Supercomputing Institute.

[1] R. D. James, J. Mech. Phys. Solids **54**, 2354 (2006).
[2] A. V. Krasheninnikov and F. Banhart, Nature Mater. **6**, 723 (2007).
[3] J. Y. Huang, S. Chen, Z. Q. Wang, K. Kempa, Y. M. Wang, S. H. Jo, G. Chen, M. S. Dresselhaus, and Z. F. Ren, Nature (London) **439**, 281 (2006).
[4] J. Y. Huang, S. Chen, Z. F. Ren, Z. Q. Wang, D. Z. Wang, M. Vaziri, Z. Suo, G. Chen, and M. S. Dresselhaus, Phys. Rev. Lett. **97**, 075501 (2006).
[5] B. I. Yakobson, Appl. Phys. Lett. **72**, 918 (1998).
[6] F. Ding, K. Jiao, M. Wu, and B. I. Yakobson, Phys. Rev. Lett. **98**, 075503 (2007).
[7] F. Ding, K. Jiao, Y. Lin, and B. I. Yakobson, Nano Lett. **7**, 681 (2007).
[8] H. Mori, S. Ogata, J. Li, S. Akita, and Y. Nakayama, Phys. Rev. B **74**, 165418 (2006).
[9] H. Mori, S. Ogata, J. Li, S. Akita, and Y. Nakayama, Phys. Rev. B **76**, 165405 (2007).
[10] J. C. Meyer, M. Paillet, and S. Roth, Science **309**, 1539 (2005).
[11] A. R. Hall, L. An, J. Liu, L. Vicci, M. R. Falvo, R. Superfine, and S. Washburn, Phys. Rev. Lett. **96**, 256102 (2006).
[12] T. Cohen-Karni, L. Segev, O. Srur-Lavi, S. R. Cohen, and E. Joselevich, Nat. Nanotechnol. **1**, 36 (2006).
[13] T. Dumitrică and R. D. James, J. Mech. Phys. Solids **55**, 2206 (2007).
[14] D.-B. Zhang, M. Hua, and T. Dumitrică, J. Chem. Phys. **128**, 084104 (2008).
[15] D.-B. Zhang and T. Dumitrică, Appl. Phys. Lett. **93**, 031919 (2008).
[16] B.-W. Jeong, J.-K. Lim, and S. B. Sinnott, J. Appl. Phys. **101**, 084309 (2007).
[17] B.-W. Jeong, J.-K. Lim, and S. B. Sinnott, Appl. Phys. Lett. **91**, 093102 (2007).
[18] B.-W. Jeong, J.-K. Lim, and S. B. Sinnott, Nanotechnology **18**, 485715 (2007).
[19] Q. Wang, Nano Lett. **9**, 245 (2009).
[20] E. Ertekin and D. C. Chrzan, Phys. Rev. B **72**, 045425 (2005).
[21] D. Porezag, Th. Frauenheim, Th. Köhler, G. Seifert, and R. Kaschner, Phys. Rev. B **51**, 12947 (1995).
[22] R. Rurali and E. Hernandez, Comput. Mater. Sci. **28**, 85 (2003).
[23] T. Dumitrică, T. Belytschko, and B. I. Yakobson, J. Chem. Phys. **118**, 9485 (2003).
[24] T. Dumitrică and B. I. Yakobson, Appl. Phys. Lett. **84**, 2775 (2004).
[25] T. Dumitrică, M. Hua, and B. I. Yakobson, Proc. Natl. Acad. Sci. U.S.A. **103**, 6105 (2006).
[26] T. Dumitrică, H. F. Bettinger, G. E. Scuseria, and B. I. Yakobson, Phys. Rev. B **68**, 085412 (2003).